

Van der Waals interaction potential between Rydberg atoms near surfaces

Johannes Block^{1,*} and Stefan Scheel¹

¹*Institut für Physik, Universität Rostock, Albert-Einstein-Strasse 23, D-18059 Rostock, Germany*

(Dated: November 27, 2017)

Van der Waals interactions, as a result of the exchange of photons between particles, can be altered by modifying the environment through which these photons propagate. As a consequence, phenomena such as the Rydberg blockade mechanism between highly excited atoms or excitons can be controlled by adding reflecting surfaces. We provide the quantum electrodynamic framework for the van der Waals interaction in the nonretarded limit that is relevant for long-wavelength transitions such as those between Rydberg systems, and show its intimate connection with common static dipole-dipole interactions, thereby providing a generalization to include macroscopic bodies.

PACS numbers: 12.20.-m, 32.80.Ee, 32.80.Xx, 34.20.Cf, 42.50.Nn

I. INTRODUCTION

Dispersion forces such as Casimir or van der Waals interactions arise from (ground-state or thermal) fluctuations of the quantized electromagnetic field that spontaneously induce a (dipole) polarization in matter. The resulting dipole-dipole interaction, e.g. between polarizable atoms, then gives rise to a typically attractive force. Early investigations focussed on fluctuating dipoles which, after the pioneering works of H.B.G. Casimir who pointed out the important role of the quantized electromagnetic field, could be traced back to its quantum electrodynamic origins. Today, we have a solid understanding of the origin of dispersion forces [1, 2] and their role in molecular and surface science [3].

Van der Waals forces, i.e. dispersion forces between atomic or molecular systems, are long-range interactions when compared to all electronic interactions such as the Pauli repulsion. However, as the van der Waals potential decays as r^{-6} at close separation, and as r^{-7} for larger distances, their effect is typically only important for (sub-)nanometer distances. An exception is the van der Waals interaction between highly excited (Rydberg) atoms that, due to the scaling of the C_6 coefficient as n^{11} with the principal quantum number n , can extend over several micrometers and cause the Rydberg blockade effect [4]. There, an atomic line is shifted out of resonance by the presence of a Rydberg atom nearby. This effect is the basis for a large number of quantum-optical protocols including the deterministic generation of single photons on demand [5] and the demonstration of a single-photon transistor [6].

The van der Waals interaction potential of ground-state atoms and molecules in the presence of arbitrary magnetodielectric bodies is well understood, and can be formulated within the framework of macroscopic quantum electrodynamics [7] as a fourth-order perturbation with respect to the single-atom electric-dipole interaction Hamiltonian [8]. For excited atoms or molecules, the shape of the interaction potential is known in the nonretarded limit, but controversial discussions remain as to its behaviour in the retarded limit [9–13], whether

the interaction remains monotonous with distance or whether it oscillates as expected from equivalent Casimir–Polder results [14, 15].

In the nonretarded limit, i.e. when the separation between the atoms or molecules is much smaller than all wavelengths associated with optical transitions in the atoms and the surrounding macroscopic bodies, the van der Waals interaction has to be taken in the static (low-frequency) limit. It is then typically computed in second-order perturbation theory with respect to the static dipole-dipole interaction Hamiltonian [16].

In this article, we will show how the static limit of the van der Waals interaction for excited atoms follows from the general fourth-order perturbation theory and, in particular, note that the distinction between nonresonant and resonant contributions to the interaction that is usually made in this context is misleading here. This derivation provides a useful generalization of the van der Waals interaction between highly excited (Rydberg) atoms near (magneto-)dielectric surfaces. As an application, we will show how the presence of boundaries, for example metallic structures for generating atom traps or confining geometries such as thin crystals, influences the blockade radius between Rydberg atoms and excitons.

The article is organized as follows: In Sec. II we derive the nonretarded limit of the van der Waals interaction potential using the formalism of macroscopic quantum electrodynamics and show how nonresonant and resonant contributions combine to add up to a generalized version of the static interaction that now also holds for arbitrary geometries. In Sec. III we provide some examples of the effects of confining geometries on the van der Waals interaction between excited atoms and excitons. In Sec. IV, we provide a numerical example of body-assisted van der Waals interaction of a pair of Rydberg atoms near a perfectly conducting mirror and discuss its influence on the Rydberg blockade mechanism.

II. VAN DER WAALS INTERACTION IN THE NONRETARDED LIMIT

The van der Waals interaction potential between two atoms prepared in energy eigenstates $|k_A\rangle$ and $|l_B\rangle$, respectively, can

*Electronic address: johannes.block@uni-rostock.de

be derived from fourth-order perturbation theory as [9]

$$\begin{aligned}
U_{AB}(\mathbf{r}_A, \mathbf{r}_B) &= \frac{i\mu_0^2}{\hbar\pi} \sum_{m \neq k, n \neq l} \frac{1}{\omega_A^{mk} + \omega_B^{nl}} \\
&\times \left\{ \mathcal{P} \int_0^\infty d\omega \frac{\omega^4 (\omega_A^{mk} + \omega_B^{nl} + \omega)}{(\omega + \omega_A^{mk})(\omega + \omega_B^{nl})} \right. \\
&+ \mathcal{P} \int_0^{-\infty} d\omega \frac{\omega^4 (\omega_A^{mk} + \omega_B^{nl} - \omega)}{(\omega - \omega_A^{mk})(\omega - \omega_B^{nl})} \left. \right\} \\
&\times [\mathbf{d}_A^{km} \cdot \mathbf{G}(\mathbf{r}_A, \mathbf{r}_B, \omega) \cdot \mathbf{d}_B^{ln}]^2 \quad (1)
\end{aligned}$$

where $\mathbf{d}_A^{km} = \langle k_A | \hat{\mathbf{d}}_A | m_A \rangle$ and ω_A^{km} denote the electric dipole moments and the transition frequencies. All information about geometric and optical properties of macroscopic bodies surrounding the atoms is contained in the dyadic Green function $\mathbf{G}(\mathbf{r}_A, \mathbf{r}_B, \omega)$ as fundamental solution of the vector Helmholtz equation

$$\nabla \times \nabla \times \mathbf{G}(\mathbf{r}, \mathbf{r}', \omega) - \varepsilon(\mathbf{r}, \omega) \frac{\omega^2}{c^2} \mathbf{G}(\mathbf{r}, \mathbf{r}', \omega) = \delta(\mathbf{r} - \mathbf{r}') \mathbf{I}. \quad (2)$$

If one or both atoms is/are initially prepared in an excited state, the integrand in Eq. (1) has poles on the real axis. Hence, using contour integration techniques, one can transform the integral along the real axis into an integral over imaginary frequencies and a sum over the residues at the poles on the real axis. In this way, a distinction into contributions from nonresonant (integral along imaginary axis) and resonant (residues) interactions can be made [17], that can partially cancel one another [14, 15]. These contributions are commonly discussed separately due to their apparently different origins. However, we will show that, in particular instances relevant to Rydberg physics, such distinction is spurious and unhelpful. Moreover, it disguises the vital connection between static and dynamic van der Waals interactions.

The physics of interactions between highly excited (Rydberg) atoms is dominated by nonretarded, i.e. static interactions due to the long transition wavelengths between neighboring Rydberg states. In the nonretarded limit, we can take the zero-frequency limit of the dyadic Green function (denoted Γ_0 in Ref. [15]) defined as

$$\Gamma_0(\mathbf{r}_A, \mathbf{r}_B) = \lim_{\omega \rightarrow 0} \frac{\omega^2}{c^2} \mathbf{G}(\mathbf{r}_A, \mathbf{r}_B, \omega). \quad (3)$$

It exists for all Green functions due to their general property [7]

$$\text{Re } \mathbf{G}(\mathbf{r}, \mathbf{r}', \omega) \stackrel{|\omega| \rightarrow 0}{\sim} \omega^{-2}, \quad \text{Im } \mathbf{G}(\mathbf{r}, \mathbf{r}', \omega) \stackrel{|\omega| \rightarrow 0}{\sim} \omega^{-1}. \quad (4)$$

Hence, in the nonretarded limit, the van der Waals interaction

potential (1) reads as

$$\begin{aligned}
U_{AB}(\mathbf{r}_A, \mathbf{r}_B) &= \frac{i}{\hbar\pi\varepsilon_0^2} \sum_{m \neq k, n \neq l} \frac{[\mathbf{d}_A^{km} \cdot \Gamma_0(\mathbf{r}_A, \mathbf{r}_B) \cdot \mathbf{d}_B^{ln}]^2}{\omega_A^{mk} + \omega_B^{nl}} \\
&\times \left\{ \mathcal{P} \int_0^\infty d\omega \frac{\omega_A^{mk} + \omega_B^{nl} + \omega}{(\omega + \omega_A^{mk})(\omega + \omega_B^{nl})} \right. \\
&+ \mathcal{P} \int_0^{-\infty} d\omega \frac{\omega_A^{mk} + \omega_B^{nl} - \omega}{(\omega - \omega_A^{mk})(\omega - \omega_B^{nl})} \left. \right\} \quad (5)
\end{aligned}$$

in which spatial dependence and frequency-dependence are decoupled and can be treated separately.

Let us focus on the frequency integral in Eq. (5) first. The double sum over all available atomic transitions determines whether resonant contributions to the van der Waals interaction potential exist. In order to determine the individual contributions of upward and downward transitions, we split the double sum into four distinct contributions

$$\sum_{m \neq k, n \neq l} \equiv \sum_{m > k, n > l} + \sum_{m < k, n > l} + \sum_{m > k, n < l} + \sum_{m < k, n < l}. \quad (6)$$

We begin with the situation that both atoms perform upward transitions ($m > k, n > l$) in which case the transition frequencies ω_A^{mk} and ω_B^{nl} are both strictly positive. Hence, the integrals along the real ω axis can be flipped to the imaginary axis, noting that the contributions from the two quarter-circles cancel one another. We thus find

$$\begin{aligned}
&\mathcal{P} \int_0^\infty d\omega \frac{\omega_A^{mk} + \omega_B^{nl} + \omega}{(\omega + \omega_A^{mk})(\omega + \omega_B^{nl})} \\
&= i \int_0^\infty d\xi \frac{\omega_A^{mk} + \omega_B^{nl} + i\xi}{(i\xi + \omega_A^{mk})(i\xi + \omega_B^{nl})}, \quad (7)
\end{aligned}$$

$$\begin{aligned}
&\mathcal{P} \int_0^{-\infty} d\omega \frac{\omega_A^{mk} + \omega_B^{nl} - \omega}{(\omega - \omega_A^{mk})(\omega - \omega_B^{nl})} \\
&= i \int_0^\infty d\xi \frac{\omega_A^{mk} + \omega_B^{nl} - i\xi}{(i\xi - \omega_A^{mk})(i\xi - \omega_B^{nl})}. \quad (8)
\end{aligned}$$

The integrations can be performed after adding both integrals with the result that

$$\begin{aligned}
&\mathcal{P} \int_0^\infty d\omega \frac{\omega_A^{mk} + \omega_B^{nl} + \omega}{(\omega + \omega_A^{mk})(\omega + \omega_B^{nl})} \\
&+ \mathcal{P} \int_0^{-\infty} d\omega \frac{\omega_A^{mk} + \omega_B^{nl} - \omega}{(\omega - \omega_A^{mk})(\omega - \omega_B^{nl})} = i\pi. \quad (9)
\end{aligned}$$

In contrast, let us investigate the contribution to the integral

from downward transitions ($m < k, n < l$). Here we write

$$\begin{aligned} & \mathcal{P} \int_0^\infty d\omega \frac{\omega_A^{mk} + \omega_B^{nl} + \omega}{(\omega + \omega_A^{mk})(\omega + \omega_B^{nl})} \\ &= -i \int_0^\infty d\xi \frac{\omega_A^{km} + \omega_B^{ln} - i\xi}{(i\xi - \omega_A^{km})(i\xi - \omega_B^{ln})} + i\pi, \end{aligned} \quad (10)$$

$$\begin{aligned} & \mathcal{P} \int_0^\infty d\omega \frac{\omega_A^{mk} + \omega_B^{nl} - \omega}{(\omega - \omega_A^{mk})(\omega - \omega_B^{nl})} \\ &= -i \int_0^\infty d\xi \frac{\omega_A^{km} + \omega_B^{ln} + i\xi}{(i\xi + \omega_A^{km})(i\xi + \omega_B^{ln})} + i\pi, \end{aligned} \quad (11)$$

where the pole contributions at $\omega = \omega_A^{km}$ and $\omega = \omega_B^{ln}$ have been added to the nonresonant contributions. Adding all up, we find that

$$\begin{aligned} & \mathcal{P} \int_0^\infty d\omega \frac{\omega_A^{mk} + \omega_B^{nl} + \omega}{(\omega + \omega_A^{mk})(\omega + \omega_B^{nl})} \\ &+ \mathcal{P} \int_0^\infty d\omega \frac{\omega_A^{mk} + \omega_B^{nl} - \omega}{(\omega - \omega_A^{mk})(\omega - \omega_B^{nl})} = -i\pi + 2i\pi = i\pi \end{aligned} \quad (12)$$

where the resonant contributions ($= 2i\pi$) overcompensate the nonresonant ones ($= -i\pi$).

Finally, the contributions to the double sum when one atom performs an upward transition and the other a downward transition ($m < k, n > l$ and $m > k, n < l$) can be written as

$$\begin{aligned} & \mathcal{P} \int_0^\infty d\omega \frac{\omega_A^{mk} + \omega_B^{nl} + \omega}{(\omega + \omega_A^{mk})(\omega + \omega_B^{nl})} \\ &+ \mathcal{P} \int_0^\infty d\omega \frac{\omega_A^{mk} + \omega_B^{nl} - \omega}{(\omega - \omega_A^{mk})(\omega - \omega_B^{nl})} \\ &= i\pi \frac{\omega_A^{km} - \omega_B^{ln}}{\omega_A^{km} + \omega_B^{ln}} + 2i\pi \frac{\omega_B^{ln}}{\omega_A^{km} + \omega_B^{ln}} = i\pi \end{aligned} \quad (13)$$

($m < k, n > l$) and

$$\begin{aligned} & \mathcal{P} \int_0^\infty d\omega \frac{\omega_A^{mk} + \omega_B^{nl} + \omega}{(\omega + \omega_A^{mk})(\omega + \omega_B^{nl})} \\ &+ \mathcal{P} \int_0^\infty d\omega \frac{\omega_A^{mk} + \omega_B^{nl} - \omega}{(\omega - \omega_A^{mk})(\omega - \omega_B^{nl})} \\ &= -i\pi \frac{\omega_A^{km} - \omega_B^{ln}}{\omega_A^{km} + \omega_B^{ln}} + 2i\pi \frac{\omega_A^{km}}{\omega_A^{km} + \omega_B^{ln}} = i\pi \end{aligned} \quad (14)$$

($m > k, n < l$), where we highlighted both nonresonant and resonant contributions.

Intriguingly, despite the fact that the frequency integrals along the real axis may or may not contain poles depending

on the nature of the atomic transition, the sum of nonresonant and resonant contributions to the integral always give identical results, with the pole contributions (over-)compensating the integrations along the imaginary axis. As a result, at least in the nonretarded limit in which frequency- and spatial dependence of the interaction potential separate, the split into nonresonant and resonant contributions is artificial and not helpful. The temperature invariance of Casimir–Polder forces in a similarly limiting regime [14, 15] is a consequence of the same type of arguments.

We are thus left with the van der Waals interaction potential in the nonretarded limit as

$$U_{AB}(\mathbf{r}_A, \mathbf{r}_B) = -\frac{1}{\hbar\epsilon_0^2} \sum_{m \neq k, n \neq l} \frac{[\mathbf{d}_A^{km} \cdot \mathbf{\Gamma}_0(\mathbf{r}_A, \mathbf{r}_B) \cdot \mathbf{d}_B^{ln}]^2}{\omega_A^{mk} + \omega_B^{nl}}. \quad (15)$$

Equation (15) can equivalently be obtained from second-order perturbation theory with the dipole-dipole interaction Hamiltonian

$$\hat{V}_{dd} = \frac{1}{\epsilon_0} \hat{\mathbf{d}}_A \cdot \mathbf{\Gamma}_0(\mathbf{r}_A, \mathbf{r}_B) \cdot \hat{\mathbf{d}}_B. \quad (16)$$

In free space, the dyadic Green function can be constructed from the static, scalar Green function

$$g_0(\mathbf{r}, \mathbf{r}') = \frac{1}{4\pi|\mathbf{r} - \mathbf{r}'|} \quad (17)$$

as

$$\mathbf{\Gamma}_0(\mathbf{r}, \mathbf{r}') = \nabla \otimes \nabla g_0(\mathbf{r}, \mathbf{r}') = -\frac{1}{4\pi} [\mathbf{I} - 3\mathbf{e}_\varrho \otimes \mathbf{e}_\varrho] \quad (18)$$

with $\varrho = \mathbf{r} - \mathbf{r}'$ and $\mathbf{e}_\varrho = \varrho/|\varrho|$, so that the dipole-dipole interaction potential takes its familiar form

$$\hat{V}_{dd} = -\frac{1}{4\pi\epsilon_0} \left[\hat{\mathbf{d}}_A \cdot \hat{\mathbf{d}}_B - 3(\hat{\mathbf{d}}_A \cdot \mathbf{e}_\varrho)(\hat{\mathbf{d}}_B \cdot \mathbf{e}_\varrho) \right]. \quad (19)$$

It is precisely this form of the interaction potential which is used in atomic physics to describe the van der Waals interaction between highly excited (Rydberg) atoms [16], if one associates the energy denominator $\hbar(\omega_A^{mk} + \omega_B^{nl})$ in Eq. (15) with the Förster defect.

III. NONRETARDED VAN DER WAALS INTERACTION IN CONFINED GEOMETRIES

The advantage of the Green function formulation of the nonretarded van der Waals interaction potential (15) becomes obvious as soon as the interacting atoms are not located in free space but in the vicinity of some macroscopic body such as trapping structures, mirrors etc. In these situations, the computation of the Green function in the nonretarded or static limit is simplified as the well-known image dipole construction applies.

As a first example, we consider two atoms in front of a perfectly reflecting mirror. By the method of images, the dyadic

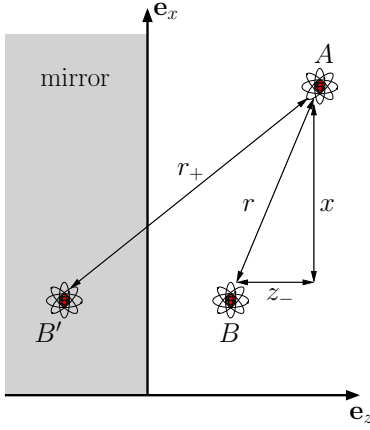


FIG. 1: Two atoms in front of perfectly conducting mirror. In case of parallel alignment we have $z_- = 0$.

Green function can be constructed from the scalar Green functions

$$g_0(\mathbf{r}, \mathbf{r}', \omega) = \frac{e^{i\omega|\mathbf{r}-\mathbf{r}'|/c}}{4\pi|\mathbf{r}-\mathbf{r}'|} \quad (20)$$

in real space and

$$g_0(\mathbf{r}, \mathbf{r}'_i, \omega) = \frac{e^{i\omega|\mathbf{r}-\mathbf{r}'_i|/c}}{4\pi|\mathbf{r}-\mathbf{r}'_i|} \quad (21)$$

in reflected space with the coordinates $\mathbf{r}'_i = (x', y', -z')$ of the image dipole as [18]

$$\mathbf{G}(\mathbf{r}, \mathbf{r}', \omega) = \left[\mathbf{I} - \frac{c^2}{\omega^2} \nabla \otimes \nabla' \right] [g_0(\mathbf{r}, \mathbf{r}', \omega) - g_0(\mathbf{r}, \mathbf{r}'_i, \omega)] + 2\mathbf{e}_z \otimes \mathbf{e}_z g_0(\mathbf{r}, \mathbf{r}'_i, \omega). \quad (22)$$

In the nonretarded (i.e. static) limit, this becomes

$$\begin{aligned} \Gamma_0(\mathbf{r}_A, \mathbf{r}_B) = & -\frac{1}{4\pi} \left[\frac{1}{r^3} \begin{pmatrix} 1 & 0 & 0 \\ 0 & 1 & 0 \\ 0 & 0 & 1 \end{pmatrix} - \frac{3}{r^5} \begin{pmatrix} x^2 & 0 & xz_- \\ 0 & 0 & 0 \\ xz_- & 0 & z_-^2 \end{pmatrix} \right] \\ & + \frac{1}{4\pi} \left[\frac{1}{r_+^3} \begin{pmatrix} 1 & 0 & 0 \\ 0 & 1 & 0 \\ 0 & 0 & 2 \end{pmatrix} - \frac{3}{r_+^5} \begin{pmatrix} x^2 & 0 & -xz_+ \\ 0 & 0 & 0 \\ xz_+ & 0 & x^2 \end{pmatrix} \right] \quad (23) \end{aligned}$$

where $x = x_A - x_B$ and $z_{\pm} = z_A \pm z_B$. The distance between the dipoles at \mathbf{r}_A and \mathbf{r}_B is denoted by r , the distance between the dipole at \mathbf{r}_B and the image dipole at \mathbf{r}'_A is r_+ (see Figure 1).

The Green function (23) thus consists of two parts, the Coulomb potential of the dipole at \mathbf{r}_B and the potential of the image dipole at \mathbf{r}'_B , both evaluated at the observation point \mathbf{r}_A . Taking the square of the Green function as necessary in Eq. (15) results in the usual interpretation of van der Waals interactions near surfaces: the interaction can be subdivided into a direct photon exchange, a photon exchange with the image dipoles, and a mixed contribution of direct and image dipole interaction.

As a result, close to a surface, the van der Waals interaction is modified according to the orientation of the dimer with respect to the surface. As a first illustrative example, in Figure 2 we show the relative strength of the van der Waals interaction for isotropically averaged dipoles near a perfectly conducting mirror. In both figures, the distance of the closest

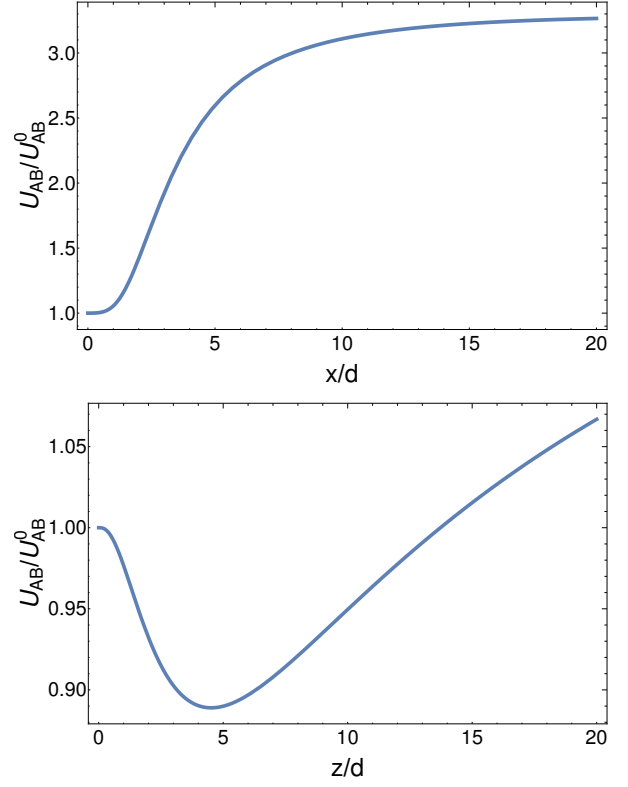


FIG. 2: Modified van der Waals interaction potential for horizontal (top) and vertical (bottom) alignment of the dimer near a perfect mirror, normalized with respect to the free-space value.

dipole from the mirror is d . The top figure refers to a horizontally aligned dimer separated by a distance x , whereas the bottom figure depicts the interaction potential of a vertically aligned dimer separated by a distance z . One observes that the van der Waals interaction between horizontally aligned Rydberg dimers can exceed their free-space value by a factor of up to 10/3 which has immediate consequences for the Rydberg blockade between atoms near surfaces as we will show later.

For real surfaces with less than unit reflectivity, the strength of the image dipole decreases by a factor equal to the (static) reflection coefficient r_p . The corresponding Green function can then be constructed from Eq. (23) by multiplying the second term in square brackets by r_p or, equivalently, by taking the nonretarded limit of the Green function presented in Appendix C of Ref. [8]. In this case, the maximal enhancement factor of horizontally aligned dimers drops to

$$\lim_{d \rightarrow 0} \frac{U_{AB}(\mathbf{r}_A, \mathbf{r}_B)}{U_{AB}^{(0)}(\mathbf{r}_A, \mathbf{r}_B)} = r_p^2 + \frac{4}{3}r_p + 1. \quad (24)$$

A. Semiconductor Rydberg excitons in finite-thickness crystals

The realm of Rydberg physics has recently been extended to include excitons in semiconductors [19], which provide a quasiparticle analogue to atoms. In this case, however, the excitons are created and thus confined in a crystal of finite thickness. Hence, the van der Waals interaction between the Rydberg excitons has to be considered inside a planar cavity (in case of the experiment reported in Ref. [19] a crystal slab of $34\mu\text{m}$ thickness). As the dominant transitions that contribute to the van der Waals interaction potential have millimeter wavelengths (the Rydberg energy of the excitons of the yellow series in Cu_2O is around 86meV), the nonretarded limit applies even for this rather thick crystal.

As the excitons are embedded in a host material, the van der Waals interaction is screened by the crystal environment. It has been shown that the local-field corrected two-point Green function is [20]

$$\mathbf{G}_{\text{loc}}(\mathbf{r}_A, \mathbf{r}_B, \omega) = \frac{3\varepsilon_A}{2\varepsilon_A + 1} \frac{3\varepsilon_B}{2\varepsilon_B + 1} \mathbf{G}(\mathbf{r}_A, \mathbf{r}_B, \omega) \quad (25)$$

with $\varepsilon_{A,B} \equiv \varepsilon(\mathbf{r}_{A,B}, \omega)$ and $\mathbf{G}(\mathbf{r}_A, \mathbf{r}_B, \omega)$ the uncorrected Green function. In the static limit, and noting that the excitons are embedded in the same crystal, we thus find that

$$\mathbf{\Gamma}_{\text{loc}}(\mathbf{r}_A, \mathbf{r}_B) = \left(\frac{3\varepsilon_{\text{Cu}_2\text{O}}}{2\varepsilon_{\text{Cu}_2\text{O}} + 1} \right)^2 \mathbf{\Gamma}_\varepsilon(\mathbf{r}_A, \mathbf{r}_B) \quad (26)$$

with the static bulk Green function inside a material with the permittivity $\varepsilon_{\text{Cu}_2\text{O}}$

$$\mathbf{\Gamma}_\varepsilon(\mathbf{r}_A, \mathbf{r}_B) = \frac{1}{\varepsilon_{\text{Cu}_2\text{O}}} \mathbf{\Gamma}_0(\mathbf{r}_A, \mathbf{r}_B). \quad (27)$$

If we choose $\varepsilon_{\text{Cu}_2\text{O}} = 7.5$, this amounts to

$$\mathbf{\Gamma}_{\text{loc}}(\mathbf{r}_A, \mathbf{r}_B) \simeq 0.26 \mathbf{\Gamma}_0(\mathbf{r}_A, \mathbf{r}_B). \quad (28)$$

In the next step, we have to include the boundaries of the planar crystal cavity. In principle, one would need to construct the dyadic Green function for a planar three-layer system as done in Ref. [21] and then take its static limit. Before we do that, we will estimate the effect of multiple scattering between the boundaries. The image of each dipole at one interface induces another image at the other interface and so on. By summing up the resulting geometric series, one finds an enhancement factor of

$$D_p \simeq [1 - r_p^+ r_p^-]^{-1} \simeq 2.4 \quad (29)$$

if we choose $\varepsilon_{\text{Cu}_2\text{O}} = 7.5$, resulting in $r_p^\pm \simeq 0.76$. It is obvious that this approach can only yield approximate results as the orientation of the dipoles inside the cavity are not taken into account.

We thus have to construct the zero-frequency limit of the known dyadic Green function for a planar three-layer system. Commonly, this is done using a two-dimensional Fourier (or Weyl) transform [1]

$$\mathbf{G}^{(S)}(\mathbf{r}, \mathbf{r}', i\xi) = \int d^2q e^{i\mathbf{q}\cdot(\mathbf{r}-\mathbf{r}')} \mathbf{G}^{(S)}(\mathbf{q}, z, z', i\xi) \quad (30)$$

with

$$\begin{aligned} \mathbf{G}^{(S)}(\mathbf{q}, z, z', i\xi) &= \frac{1}{8\pi^2 b} \sum_{\sigma=s,p} \left\{ \frac{r_\sigma^+ r_\sigma^- e^{-2bd}}{D^\sigma} \right. \\ &\times \left[\mathbf{e}_\sigma^+ \otimes \mathbf{e}_\sigma^+ e^{-b(z-z')} + \mathbf{e}_\sigma^- \otimes \mathbf{e}_\sigma^- e^{-2bd+b(z-z')} \right] \\ &\left. + \frac{1}{D^\sigma} \left[\mathbf{e}_\sigma^+ \otimes \mathbf{e}_\sigma^- r_\sigma^- e^{-b(z+z')} + \mathbf{e}_\sigma^- \otimes \mathbf{e}_\sigma^+ r_\sigma^+ e^{-2bd+b(z+z')} \right] \right\} \quad (31) \end{aligned}$$

as the Weyl components of the Green tensor. The r_σ^\pm are the Fresnel reflection coefficients at the upper and lower crystal-air interface, respectively. The function $D^\sigma = 1 - r_\sigma^- r_\sigma^+ e^{-2bd}$ accounts for multiple reflections.

In this notation, \mathbf{q} denotes the in-plane wavevector components and $b = \sqrt{\xi^2/c^2\varepsilon(i\xi) + q^2}$ its component normal to the planar surfaces. In view of the nonretarded limit, we can set $b \simeq q$. In the same limit, only the p -polarized waves will contribute, hence we set $\sigma = p$ with

$$\begin{aligned} \mathbf{e}_p^\pm &= \mp \frac{b}{\kappa} [\cos\varphi \mathbf{e}_x + \sin\varphi \mathbf{e}_y] - \frac{iq}{\kappa} \mathbf{e}_z \\ &\simeq -\frac{q}{\kappa} [\pm \cos\varphi \mathbf{e}_x \pm \sin\varphi \mathbf{e}_y + i\mathbf{e}_z]. \quad (32) \end{aligned}$$

We restrict ourselves to the case in which the excitons are created at $z = z'$. The coordinate system is oriented such that $\mathbf{r} - \mathbf{r}'$ points along the x -axis, hence $\mathbf{q} \cdot (\mathbf{r} - \mathbf{r}') = qx \cos\varphi$.

Expanding out the dyadic products of polarization unit vectors and using the integral representation of the Bessel functions, one finds

$$\begin{aligned} &\int_0^{2\pi} d\varphi e^{iqx \cos\varphi} [\mathbf{e}_p^+ \otimes \mathbf{e}_p^+ + \mathbf{e}_p^- \otimes \mathbf{e}_p^-] \\ &= \frac{2\pi q^2}{\kappa^2} \begin{pmatrix} J_0(qx) - J_2(qx) & 0 & 0 \\ 0 & J_0(qx) + J_2(qx) & 0 \\ 0 & 0 & -2J_0(qx) \end{pmatrix} \quad (33) \end{aligned}$$

and

$$\begin{aligned} &\int_0^{2\pi} d\varphi e^{iqx \cos\varphi} \mathbf{e}_p^\pm \otimes \mathbf{e}_p^\mp \\ &= -\frac{\pi q^2}{\kappa^2} \begin{pmatrix} J_0(qx) - J_2(qx) & 0 & \pm 2J_1(qx) \\ 0 & J_0(qx) + J_2(qx) & 0 \\ \mp 2J_1(qx) & 0 & -2J_0(qx) \end{pmatrix}. \quad (34) \end{aligned}$$

The remaining q -integrals can be performed by expanding the Bessel functions into power series and using ($r_- = r_+ \equiv r$)

$$\int_0^\infty dq \frac{q^n}{1 - r^2 e^{-2qd}} = \frac{n!}{(2d)^{n+1}} \text{Li}_{n+1}(r^2), \quad (35)$$

$$\int_0^\infty dq \frac{e^{-2qz} q^n}{1 - r^2 e^{-2qd}} = \frac{n!}{(2d)^{n+1}} \Phi_{n+1}(r^2, z/d), \quad (36)$$

$$\int_0^\infty dq \frac{e^{-2q(d-z)} q^n}{1 - r^2 e^{-2qd}} = \frac{n!}{(2d)^{n+1}} \Phi_{n+1}(r^2, 1 - z/d), \quad (37)$$

where $\text{Li}_n(x)$ is the polylogarithm function and $\Phi_n(x, z)$ the Lerch Phi function. These special functions are very well approximated by

$$\text{Li}_n(r^2) \simeq r^2, \quad \Phi_n(r^2, z/d) \simeq (d/z)^n, \quad n \geq 3, \quad (38)$$

with errors less than 2.5%. We can identify two types of integrals,

$$I_m = \int_0^\infty dq \frac{r^2 e^{-2qd}}{1 - r^2 e^{-2qd}} q^2 J_m(qx) \simeq \frac{(m+2)!}{m!} \left(\frac{x}{4d}\right)^m \times \frac{r^2}{(2d)^3} {}_2F_1\left(\frac{m+3}{2}, \frac{m+4}{2}, m+1, -\frac{x^2}{4d^2}\right), \quad (39)$$

$$\tilde{I}_m = \int_0^\infty dq \frac{r e^{-2qz}}{1 - r^2 e^{-2qd}} q^2 J_m(qx) \simeq r \frac{(m+2)!}{m!} \left(\frac{x}{4z}\right)^m \times \frac{1}{(2d)^3} {}_2F_1\left(\frac{m+3}{2}, \frac{m+4}{2}, m+1, -\frac{x^2}{4z^2}\right), \quad (40)$$

with the help of which we can express the dyadic Green function in the required nonretarded limit. In the simplest case in which the excitons are excited halfway between the plate interfaces, $z = d/2$, we find

$$4\pi\kappa^2 \mathbf{G}^{(S)}(\mathbf{r}, \mathbf{r}', i\xi) \simeq \text{diag}(I_0 - I_2 - \tilde{I}_0 + \tilde{I}_2, I_0 + I_2 - \tilde{I}_0 - \tilde{I}_2, -2I_0 - 2\tilde{I}_0). \quad (41)$$

Inserted into the expression for the van der Waals potential and normalizing with respect to the local-field corrected bulk value, we find the enhancement factor due to the presence of the boundaries as shown in Fig. 3. There we show

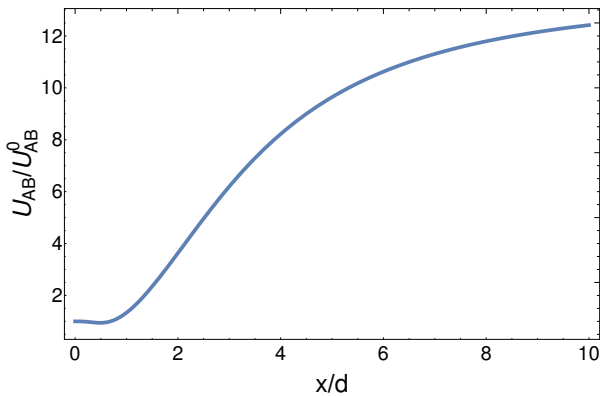


FIG. 3: Enhancement factor of the van der Waals interaction potential between excitons separated by a distance x inside a bulk Cu_2O crystal with thickness d .

the enhancement of the nonretarded van der Waals interaction

between two excitons located inside a crystal of thickness d at a vertical position $z = d/2$, and separated by a horizontal distance x . Note that, due to the lack of any other length scale in the considered nonretarded limit, the figure can be scaled to arbitrary values of x and d , as they are the only remaining length scales in the system. We see that, depending on the ratio x/d , the enhancement of the van der Waals potential due to the restricted geometry can easily exceed factors of 5 or more.

This explains why the theoretical values of the Rydberg blockade efficiency given in Ref. [19] differ substantially from the data extracted from the experiment. The crystal thickness was given as $d = 34\mu\text{m}$, and the Rydberg blockade radius estimated to be around $30\mu\text{m}$. The enhancement factor can therefore be estimated to be around 2, which accounts for the discrepancy between theory and experiment in Ref. [19].

IV. RYDBERG ATOMS IN FRONT OF A PERFECTLY CONDUCTING PLATE

We will now apply the concepts described above to the van der Waals interaction of Rydberg atoms close to a perfect mirror, which can be viewed as a model system for a superconducting strip line cavity [22] or similar surfaces [23, 24]. Two modifications are required to the simple perturbative model. First, nondegenerate perturbation theory fails when describing interactions between two Rydberg states [25] as the Förster defect [16] can become very small for resonant interactions. Hence, it becomes necessary to exactly diagonalize the van der Waals interaction Hamiltonian. Second, the spatial extent of the wavefunction of a Rydberg atom requires the inclusion of higher-order multipole moments of the interaction [26].

Including higher-order terms up to quadrupole-quadrupole interaction, the interaction Hamiltonian then reads

$$\begin{aligned} \hat{H}_{int} = & \hat{\mathbf{d}}_A \cdot \mathbf{\Gamma}_0(\mathbf{r}_A, \mathbf{r}_B) \cdot \hat{\mathbf{d}}_B \\ & + \hat{\mathbf{d}}_A \cdot \mathbf{\Gamma}_0(\mathbf{r}_A, \mathbf{r}_B) \overleftrightarrow{\nabla}_B : \hat{\mathbf{Q}}_B \\ & + \hat{\mathbf{Q}}_A : \overleftrightarrow{\nabla}_A \mathbf{\Gamma}_0(\mathbf{r}_A, \mathbf{r}_B) \cdot \hat{\mathbf{d}}_B \\ & + \hat{\mathbf{Q}}_A : \overleftrightarrow{\nabla}_A \mathbf{\Gamma}_0(\mathbf{r}_A, \mathbf{r}_B) \overleftrightarrow{\nabla}_B : \hat{\mathbf{Q}}_B \end{aligned} \quad (42)$$

where indices and arrows on the gradient operator indicate the spatial coordinate and the tensor index with respect to which the differentiation is performed. Here, the (tensorial) quadrupole moment operators are denoted by $\hat{\mathbf{Q}}_{A,B}$, and the notation $:$ indicates the contraction of two indices (Hadamard product).

In order to calculate the gradient of the static Green function for a perfect mirror, Eq. (23), it is convenient to define a matrix $\mathbf{A} = \overleftrightarrow{\nabla}_r \frac{\mathbf{r}}{r}$ with $\mathbf{r} = \mathbf{r}_A - \mathbf{r}_B$. For the free-space part $\mathbf{\Gamma}_0^{\text{fs}}$, we can then write

$$\begin{aligned} \overleftrightarrow{\nabla}_A \mathbf{\Gamma}_0^{\text{fs}}(\mathbf{r}, \omega) = & \frac{1}{4\pi} \left\{ \frac{3}{r^4} \mathbf{e}_r \otimes \mathbf{I} - \frac{9}{r^4} \mathbf{e}_r \otimes \mathbf{e}_r \otimes \mathbf{e}_r \right. \\ & \left. + \frac{3}{r^3} (\mathbf{A} \otimes \mathbf{e}_r + A_{ik} e_{rj}) \right\} \end{aligned} \quad (43)$$

and

$$\begin{aligned} \Gamma_0^{\text{fs}}(\mathbf{r}, \omega) \overleftarrow{\nabla}_B = & \frac{c^2}{4\pi\omega^2} \left\{ -\frac{3}{r^4} \mathbf{I} \otimes \mathbf{e}_r + \frac{9}{r^4} \mathbf{e}_r \otimes \mathbf{e}_r \otimes \mathbf{e}_r \right. \\ & \left. + \frac{3}{r^3} (\mathbf{e}_r \otimes \mathbf{A} + A_{ik} e_{rj}) \right\}. \end{aligned} \quad (44)$$

This means that the double gradient of the nonretarded Green function required for the quadrupole-quadrupole interaction becomes

$$\begin{aligned} \overrightarrow{\nabla}_A \Gamma_0^{\text{fs}}(\mathbf{r}, \omega) \overleftarrow{\nabla}_B = & \frac{c^2}{4\pi\omega^2} \\ & \times \left\{ \frac{12}{r^5} \mathbf{e}_r \otimes \mathbf{I} \otimes \mathbf{e}_r - \frac{36}{r^5} \mathbf{e}_r \otimes \mathbf{e}_r \otimes \mathbf{e}_r \otimes \mathbf{e}_r \right. \\ & + \frac{3}{r^4} (3A_{ij} e_{rk} e_{rl} + 3A_{ik} e_{rj} e_{rl} + 3A_{il} e_{rj} e_{rk} - A_{il} \delta_{jk}) \\ & \left. + \frac{3}{r^3} (A_{ik} A_{jl} + A_{ij} A_{kl} - 3e_{r_i} A_{jl} e_{r_k} - 3e_{r_i} e_{r_j} A_{kl}) \right\}. \end{aligned} \quad (45)$$

The scattering part of the tensor, corresponding to the second line in Eq. (23), is calculated accordingly.

The interaction Hamiltonian is then expanded into a basis spanned by the states $|\psi\rangle = |n, l, j, m_j\rangle$ where n is the principal quantum number, l is the angular momentum quantum number, the total angular momentum $j = l \pm \frac{1}{2}$ accounts for the spin, and $m_j \in [-j, j]$ is the projection of j onto the quantization axis. The binding energies are determined via the quantum defect δ_{nlj} and the modified Rydberg series

$$E_{n,l,j} = -\frac{E_{\text{Ry}}}{(n - \delta_{nlj})^2}. \quad (46)$$

Quantum defects for rubidium Rydberg states with $n > 11$ were calculated in Refs. [27, 28], whereas for $n < 11$, data can be found in Ref. [29]. Detailed measurements of absolute excitation energies with extracted quantum defects can be found in Ref. [30].

The quadrupole operator is defined as $\hat{Q} = \frac{q}{2} \hat{\mathbf{r}} \otimes \hat{\mathbf{r}}$ and can be expressed in terms of spherical harmonics [26]. The radial part of both $\hat{\mathbf{d}}$ and \hat{Q} , i.e. the matrix elements $\langle n, l, j | \hat{r} | n', l', j' \rangle$ and $\langle n, l, j | \hat{r}^2 | n', l', j' \rangle$, respectively, are calculated numerically using Numerov's method integrating inward until an inner cutoff point. For the angular components, we use the Wigner-Eckart theorem to write

$$\begin{aligned} \langle l, j, m_j | Y_{kq} | l', j', m'_j \rangle = & (-1)^{j+j'-m_j+k+\frac{1}{2}} \\ & \times \sqrt{\frac{(2j+1)(2j'+1)(2l+1)(2l'+1)(2k+1)}{4\pi}} \\ & \times \begin{pmatrix} j & k & j' \\ -m & q & m' \end{pmatrix} \begin{pmatrix} l & k & l' \\ 0 & 0 & 0 \end{pmatrix} \left\{ \begin{matrix} l & j & \frac{1}{2} \\ j' & l' & k \end{matrix} \right\}, \end{aligned} \quad (47)$$

where we set $s = s' = \frac{1}{2}$ and use the Wigner-3j-symbol $\begin{pmatrix} l & l' & L \\ m & m' & M \end{pmatrix}$ as well as the Wigner-6j-symbol $\left\{ \begin{matrix} l & j & s \\ j' & l' & k \end{matrix} \right\}$.

Now we turn to a setup of two atoms in parallel alignment in front of a perfect mirror, see Fig. 1 with $z_- = 0$. In free

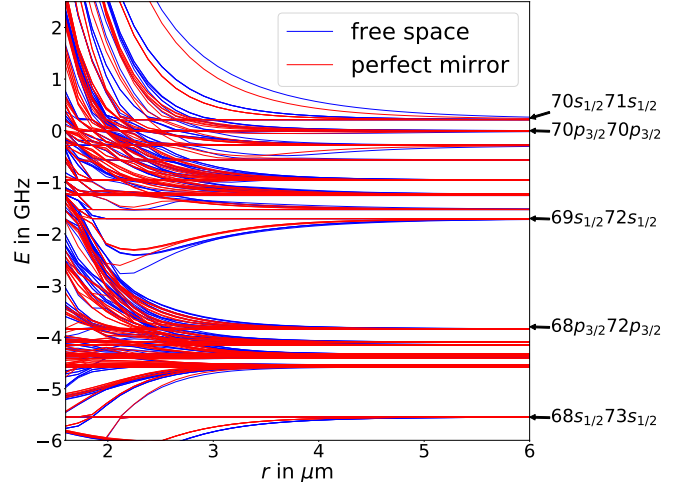


FIG. 4: We depict the interaction potential of several states around the Rubidium $70p_{3/2}70p_{3/2}$ asymptote at 0 GHz. Blue lines: free-space interaction. Red lines: interaction of two atoms in parallel alignment at a distance $d \approx 1 \mu\text{m}$ in front of a perfect mirror.

space, due to isotropy one can always choose the quantization axis of the atoms to be parallel to the the intermolecular axis connecting both atoms. This implies a conservation of the total projection of the angular momentum $M = m_A + m_B$. Thus, the interaction Hamiltonian decomposes into blocks of constant M [16] which simplifies the computation considerably.

The presence of a macroscopic body breaks that isotropy and hence the conservation of $M = m_A + m_B$. Therefore, one has to include a far larger basis set for the full diagonalization. In Ref. [25], the authors considered two Rb atoms in states $70p + 70p$, and focussed on very few strongly dipole- and quadrupole-coupled asymptotes for the diagonalization, resulting in a basis set of 142 two-atom states, i.e. a 142×142 matrix that had to be diagonalized. Breaking isotropy by introducing a macroscopic body immediately generates a 700×700 -matrix. In general, convergence for free-space dipole-dipole interaction of Rydberg atoms is often only achieved with a basis set of 4000 to 6000 states [31].

In Fig. 4, we present an example of the effects of a nearby surface on the van der Waals interaction between two Rydberg atoms. Here, we take into account the same basis set as in Ref. [25], including hyperfine splitting for d - and f -states. We use the the *gerade* symmetrization, i.e. $|A, B\rangle \rightarrow \frac{1}{\sqrt{2}} (|A, B\rangle - (-1)^{l_A+l_B} |B, A\rangle)$ for a two-atom state $|A, B\rangle = |n_A l_A j_A m_{j,A}; n_B l_B j_B m_{j,B}\rangle$. We show the interaction of two Rb atoms in free space (blue) and at a distance of $\sim 1 \mu\text{m}$ from a perfectly reflecting mirror (red). One observes notable changes in the interaction potential for interatomic distances $r < 3.5 \mu\text{m}$.

As illustrative examples, We will investigate the $70s_{1/2}71s_{1/2}$ and $69s_{1/2}72s_{1/2}$ asymptotes further. Both potential curves are fitted to a C_6/r^6 potential as expected from the nonretarded van der Waals interaction. This can only be a rough estimate since we also consider multipole

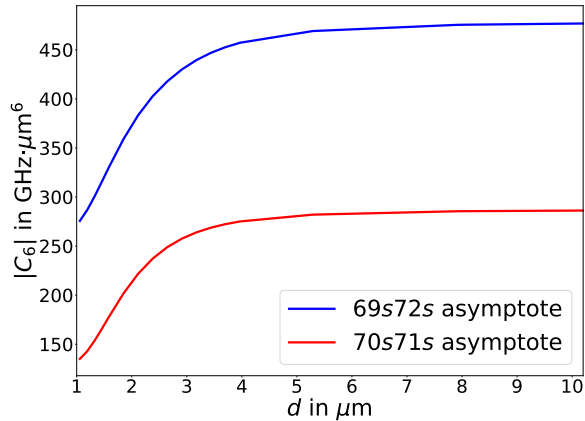


FIG. 5: Development of the C_6 coefficient over distance d between the atoms and the perfect mirror.

interactions up to quadrupole-quadrupole that lead to additional terms in the potential. We find a general decrease in the C_6 coefficient with smaller distance d between the atoms and the perfect mirror. Results are shown in Figure 5. For the $70s_{1/2}71s_{1/2}$ asymptote, the free space coefficient is approximately $C_6^{\text{fs}} \approx 287 \text{ GHz} \cdot \mu\text{m}^6$ while at a distance $d \approx 1 \mu\text{m}$ it reduces to $C_6^{\text{mirror}}(d \approx 1 \mu\text{m}) \approx 152 \text{ GHz} \cdot \mu\text{m}^6$. For the $69s_{1/2}72s_{1/2}$ asymptote, we can extract $C_6^{\text{fs}} \approx 478 \text{ GHz} \cdot \mu\text{m}^6$ and $C_6^{\text{mirror}}(d \approx 1 \mu\text{m}) \approx 283 \text{ GHz} \cdot \mu\text{m}^6$.

V. CONCLUSIONS

The quantum electrodynamic approach to van der Waals interactions provides one with the notion of an exchange of virtual photons as the cause of that fluctuation-induced interaction. For atoms in excited states, the exchange of real photons contributes, too. We have shown here that, in the nonretarded limit, the contributions from virtual and real photons, i.e. the nonresonant and resonant contributions to the van der Waals potential, overcompensate one another to the extent that a distinction between them looks entirely artificial. However, it should be stressed that this is only true in the nonretarded limit in which the spatial dependence that resides in the dyadic Green function, factorizes from the frequency dependence.

The immediate result is that, perhaps unsurprisingly, in this limit, the quantum electrodynamic calculation coincides with the static dipole-dipole interaction commonly used in atomic Rydberg physics. However, the more general quantum electrodynamic approach provides one with the additional insight how macroscopic bodies alter the van der Waals interaction between highly excited atoms. For Rydberg atoms, it is easy to envisage situations in which the body-induced modification of the van der Waals potential can be significant. Indeed, as soon as the atom-surface distance becomes comparable to the interatomic separation, one has to expect contributions to the interaction potential that arises from the reflection of the photons off the body surface.

We have shown how to construct the van der Waals potential near a planar interface as well as inside a planar waveguide, and given an estimate of the enhancement factor of the van der Waals interaction of excitons in a thin crystal. Note, however, that in this specific example we only investigated the perturbative interaction that does not take degeneracies into account. Also, we have disregarded the absolute strength of the interaction which would require a detailed description of the transition dipole moments of the exciton states. This will be the subject of future work.

For Rydberg atoms near planar interfaces such as superconducting striplines, the direct diagonalization approach is more involved than in free space as the presence of the interface breaks the isotropy of space. This implies that the interaction Hamiltonian does no longer decompose into blocks with constant total magnetic quantum number as quantization axis and intermolecular axis no longer necessarily coincide. We have given an example of an Rb dimer horizontally aligned to a perfect conductor to illustrate the effect of the interface on the van der Waals potential and subsequently on the Rydberg blockade radius. With this, it is now possible to use macroscopic bodies as additional tuning devices for controlling interactions of Rydberg systems.

Acknowledgments

We gratefully acknowledge discussions with R. Schmidt. This work was partially supported by the Collaborative Research Centre SFB 652/3 'Strong correlations in the radiation field' funded by the Deutsche Forschungsgemeinschaft and the Landesgraduiertenförderung Mecklenburg-Vorpommern.

[1] S.Y. Buhmann, *Dispersion forces I: Macroscopic Quantum Electrodynamics and Ground-State Casimir, Casimir-Polder and van der Waals Forces* (Springer, Berlin, 2012).
 [2] A. Salam, *Molecular quantum electrodynamics* (Wiley, Hoboken, 2010).
 [3] J.N. Israelachvili, *Intermolecular and surface forces* (Academic Press, Amsterdam, 2007).
 [4] M. Lukin, M. Fleischhauer, R. Côté, L. Duan, D. Jaksch, J. Cirac, and P. Zoller, *Dipole blockade and quantum infor-*

mation processing in mesoscopic atomic ensembles, Phys. Rev. Lett. **87**, 037901 (2001).
 [5] Y.O. Dudin and A. Kuzmich, *Strongly interacting Rydberg excitations of a cold atomic gas*, Science **336**, 887 (2012).
 [6] D. Tiarks, S. Baur, K. Schneider, S. Dürr, and G. Rempe, Phys. Rev. Lett. **113**, 053602 (2014).
 [7] S. Scheel and S.Y. Buhmann, *Macroscopic quantum electrodynamics — concepts and applications*, Acta Physica Slovaca **58**, 675 (2008).

- [8] H. Safari, S.Y. Buhmann, D.-G. Welsch, and Ho Trung Dung, *Body-assisted van der Waals interaction between two atoms*, Phys. Rev. A **74**, 042101 (2006).
- [9] H. Safari and M.R. Karimpour, *Body-Assisted van der Waals Interaction between Excited Atoms*, Phys. Rev. Lett. **114**, 013201(2015).
- [10] L. Gomberoff, R.R. McLone, and E.A. Power, *Long-Range Retarded Potentials between Molecules*, J. Chem. Phys. **44**, 4148 (1966).
- [11] E.A. Power and T. Thirunamachandran, *Dispersion forces between molecules with one or both molecules excited*, Phys. Rev. A **51**, 3660 (1995).
- [12] M. Donaire, R. Guérout, and A. Lambrecht, *Quasi-resonant van der Waals interaction between non-identical atoms*, Phys. Rev. Lett. **115**, 033201 (2015).
- [13] P. Barcellona, R. Passante, L. Rizzuto, and S.Y. Buhmann, *van der Waals interactions between excited atoms in generic environments*, Phys. Rev. A **94**, 012705 (2016).
- [14] S.Å. Ellingsen, S.Y. Buhmann, and S. Scheel, *Temperature-Independent Casimir-Polder Forces Despite Large Thermal Photon Numbers*, Phys. Rev. Lett. **104**, 223003 (2010).
- [15] S.Å. Ellingsen, S.Y. Buhmann, and S. Scheel, *Temperature-independent Casimir-Polder forces in arbitrary geometries*, Phys. Rev. A **84**, 060501(R) (2011).
- [16] T.G. Walker and M. Saffman, *Consequences of Zeeman degeneracy for the van der Waals blockade between Rydberg atoms*, Phys. Rev. A **77**, 032723 (2008).
- [17] S.Y. Buhmann, L. Knöll, D.-G. Welsch, and Ho Trung Dung, *Casimir-Polder forces: A nonperturbative approach*, Phys. Rev. A **70**, 052117 (2004).
- [18] C.T. Tai, *Dyadic Green functions in electromagnetic theory* (IEEE Press, Piscataway, 1994).
- [19] T. Kazimierzczuk, D. Fröhlich, S. Scheel, H. Stolz, and M. Bayer, *Giant Rydberg excitons in the semiconductor Cu₂O*, Nature **514**, 343 (2014).
- [20] Ho Trung Dung, S.Y. Buhmann, and D.-G. Welsch, Phys. Rev. A **74**, 023803 (2006).
- [21] M.S. Tomaš, *Green function for multilayers: Light scattering in planar cavities*, Phys. Rev. A **51**, 2545 (1995).
- [22] H. Hattermann, D. Bothner, L.Y. Ley, B. Ferdinand, D. Wiedmaier, L. Sárány, R. Kleiner, D. Koelle, and J. Fortágh, *Coupling ultracold atoms to a superconducting coplanar waveguide resonator*, arXiv:1707.02730.
- [23] T. Thiele, S. Filipp, J.A. Agner, H. Schmutz, J. Deiglmayr, M. Stammeier, P. Allmendinger, F. Merkt and A. Wallraff, Phys. Rev. A **90**, 013414 (2014).
- [24] P. Weiss, M. Knufinke, S. Bernon, D. Bothner, L. Sárány, C. Zimmermann, R. Kleiner, D. Koelle, J. Fortágh and H. Hattermann, Phys. Rev. Lett. **114**, 113003 (2015).
- [25] J. Stanovevic, R. Côté, D. Tong, E.E. Eyler, and P.L. Gould, Phys. Rev. A **78**, 082709 (2008).
- [26] J.A. Crosse, S.A. Ellingsen, K. Clements, S.Y. Buhmann, and S. Scheel, Phys. Rev. A **82**, 010901 (2010).
- [27] W. Li, I. Mourachko, M.W. Noel, and T.F. Gallagher, Phys. Rev. A **67**, 052502 (2003).
- [28] J. Han, Y. Jamil, D.V.L. Norum, P.J. Tanner, and T.F. Gallagher, Phys. Rev. A **74**, 054502 (2006).
- [29] J.E. Sansonetti, Journal of Physical and Chemical Reference Data **35**, 301 (2006); J.E. Sansonetti, Journal of Physical and Chemical Reference Data **37**, 1183 (2008).
- [30] M. Mack, F. Karlewski, H. Hattermann, S. Höckh, F. Jessen, D. Cano, and J. Fortágh, Phys. Rev. A **83**, 052515 (2015).
- [31] J.S. Cabral, J.M. Kondo, L.F. Gonçalves, V.A. Nascimento, L.G. Marcassa, D. Booth, J. Tallant, A. Schwettmann, K.R. Overstreet, J. Sedlacek, and J.P. Shaffer, J. Phys. B: At. Mol. Opt. Phys. **44**, 184007 (2011).